Innovation-based Methods for Estimating Observation Error Variances During Ensemble Data Assimilation

Henry Santer, [a] Jonathan Poterjoy, [a] Mohamad El Gharamti, [b]

[a] *Department of Atmospheric and Oceanic Science, University of Maryland, College Park*

[b] *National Center for Atmospheric Research, Boulder, Colorado*

Corresponding author: Henry Santer, hsanter@umd.edu

ABSTRACT: Many data assimilation methods require knowledge of the first two moments of the background and observation errors to function optimally. To ensure the effective performance of such methods, it is often advantageous to estimate the second moment of the observation errors directly. We examine three different strategies for doing so, focusing specifically on the case of a single scalar observation error variance parameter r. The first method is the well-known Desroziers ”diagnostic check” iteration. The second method, described in Karspeck (2016), generates a point estimate of r by taking the expectation of various observation-space statistics and using an ensemble to model background error statistics explicitly. The third method is an approximate Bayesian scheme that uses an inverse-gamma prior and a modified Gaussian likelihood. All three methods can recover the correct observation error variance when the observation error is Gaussian. We also demonstrate that it is often possible to estimate r even when the observation error is not Gaussian, or when the forward operator mapping model states into observation space is nonlinear. The Desroziers method is found to be most robust to these complications; however, the other two methods perform similarly well in most cases and have the added benefit that they can be used to estimate r before data assimilation. We conclude that further investigation is warranted into the latter two methods, specifically into how they perform when extended to the multivariate case.

SIGNIFICANCE STATEMENT: Observations of the Earth system (e.g. from satellites, radiosondes, aircraft, etc.) each have some associated uncertainty. In order to use observations to improve model forecasts, it is important to understand the size of that uncertainty. This study compares three statistical methods for estimating how large observation errors tend to be, all of which can be continuously implemented whenever new observations are used to correct a model. Our results suggest that all three methods can improve forecast outcomes, but that, if observations are believed to have highly biased or skewed errors, care should be taken in choosing which to use and interpreting its results. Future studies should investigate robust methods for estimating more complicated types of errors.

1. Introduction

A common challenge across a range of scientific disciplines is generating a *best estimate* of the state of some system given multiple sources of information about it. The atmosphere and oceans are notable examples of such systems — where the associated state is described by values of temperature, pressure, salinity, fluid motion, etc. over a large domain — but many more instances of the state estimation problem exist across geoscience and engineering. Data assimilation performs state estimation by combining forecasts from a numerical model with observations of the system. In order to work effectively, many data assimilation methods require knowledge of the second moments of the background and observation errors. These are usually given by the background error covariance matrix $\mathbf{B}$ and the observation error covariance matrix $\mathbf{R}$, respectively. Tandeo et al. (2020) describes a range of issues that can occur if either or both of $\mathbf{B}$ or $\mathbf{R}$ is specified incorrectly during data assimilation. In particular, they show that the values used for each matrix during data assimilation must match the true uncertainty in the background and observations in order to obtain an analysis that is closest to the true state and free of extraneous noise. In practice, the exact values of $\mathbf{B}$ and $\mathbf{R}$ can never be exactly known, just as the true state can never be exactly known. Accordingly, a large body of data assimilation research is dedicated to modeling the background and observation errors in conjunction with estimating the state; see challenges outlined recently in Walsworth et al. (2023). The present article focuses on methods for modeling $\mathbf{R}$, specifically in the case of uncorrelated scalar observations. Additionally, we leverage large ensemble sizes for each model and forego any adaptive inflation strategies to avoid issues associated with estimating **R** and **B** concurrently.

The ”observation error” that is usually considered for data assimilation purposes is, in reality, the result of multiple distinct sources of error. These include 1) errors in the accuracy/precision of observing instruments; 2) ”representativeness” errors that arise from the truncation of scales when discretizing the system of interest; and 3) errors in the forward operator h, which relates the model state to observations (Janjić et al. 2018). Note that h is often itself linear or linearized about some point; in either case, we use **H** to denote the corresponding tangent linear operator for h. In practice, it is difficult to separate the observation error into distinct components, so we generally treat it as a single random variable, whose covariance matrix is **R**.

Estimation of **R** during data assimilation is almost always accomplished by examining *innovation statistics*, defined as the difference between ingested observations and their corresponding model estimates before and after data assimilation. Dee (1997) uses background innovations to estimate model and observation error statistics based on a simple iterative maximum likelihood approach. Desroziers and Ivanov (2001) introduces an alternate iterative scheme that relies on both background and analysis innovations to estimate error statistics. Perhaps the most widely known method for jointly estimating background and observation error statistics is the posterior ”consistency check” described in Desroziers et al. (2005) (hereafter D05). The key result is that, if background and observation error statistics are properly specified to begin with, taking statistical expectations of different products of background and analysis innovations allows one to recover those correct error statistics. Even if the initially specified background and observation error statistics are not correct, this process can be iterated to create continuously evolving estimates of **B** and **R** as more and more observations are assimilated. Ménard et al. (2009) describes the convergence of this iterative approach when either or both of the background and observation error variance are incorrectly specified. The D05 scheme has been implemented for data assimilation systems of complexity ranging from simple idealized models to complex models used for operational environmental prediction. Additionally, the scheme can be used either in an ”offline” way — accumulating a large number of observations from which to create a single, time-independent estimate of error statistics — or in an ”online” way, in which the estimation is done intermittently as new observations are ingested to allow the estimates to vary over time. In the latter case, it is useful to apply some temporal smoothing to the time series of estimates to reduce the effects of sampling noise from one estimate to the next (Li et al. 2009; Miyoshi et al. 2013). Finally, a related but distinct approach to the D05 method is to take the expectation of only background innovations to estimate the total innovation variance $\mathbf{HBH^T} + \mathbf{R}$, and then use an ensemble to directly estimate $\mathbf{HBH^T}$, the background error variance projected into observation space. The difference between these two estimates provides an estimate of $\mathbf{R}$. This is the method described in Karspeck (2016) (hereafter K16). We make the connection between the D05 method and the K16 method explicit in section 3.

All of the above methods yield point estimates of $\mathbf{R}$, sometimes without an accompanying measure of the uncertainty surrounding the estimate. An alternative approach is to parameterize variances and correlations in $\mathbf{R}$ and use Bayes' Theorem to maintain a distributional estimate for the parameters that becomes updated recursively as new observations are ingested. To do so, it is necessary to specify an initial prior distribution for the parameter or parameters. Stroud and Bengtsson (2007) (hereafter SB07) uses an inverse-gamma prior distribution to model an inflation parameter for $\mathbf{R}$. Inverse-gamma distributions are an attractive choice for modeling variance parameters because they only support positive values, removing the need for heuristics to prevent an estimated variance from taking on negative values (Gharamti 2018). However, SB07 simultaneously scales the model error covariance matrix $\mathbf{Q}$ with the same inflation parameter, effectively fixing the $\mathbf{Q}$ to always be a constant scalar multiple of $\mathbf{R}$. Stroud et al. (2018) provides a more general framework for Bayesian parameter estimation that allows for Gaussian or nonparametric prior distributions. In section 3, we introduce a variation of the Stroud et al. (2018) method that takes advantage of an inverse-gamma prior without imposing any of the additional assumptions made by the SB07 method.

The objective of this paper is to compare three different methods for estimating a scalar observation error variance: the D05 method, the K16 method, and the Bayesian inverse-gamma method described below. The remaining sections are organized as follows. Section 2 provides an overview of the data assimilation framework we use and defines notation for the remainder of the paper. Section 3 describes the three observation error variance estimation methods in detail. Section 4 introduces the models and experimental setups we use to compare the three methods, and Section 5 discusses the results of those experiments. Conclusions and final thoughts are presented in Section 6.

2. Overview of Ensemble Data Assimilation and Notation

Consider a discrete-time model for the evolution of some geophysical system, given by the equation

$$\mathbf{x}_k = M(\mathbf{x}_{k-1}) + \eta_k, \tag{1}$$

where $\mathbf{x}_k$ denotes the model state at time k, η_k is the model error, and M represents the system dynamics. At each time, a p-dimensional observation $\mathbf{y}_k^o$ of the system is taken. Let $\mathbf{Y}_k^o = \{\mathbf{y}_k^o, \mathbf{y}_{k-1}^o, \ldots \mathbf{y}_1^o, \mathbf{y}_0^o\}$ denote the collection of all observations ingested up until the current time. To compare the model state to observations, it is necessary to consider it in observation space. Let h be the forward operator that accomplishes this; we then have

$$\mathbf{y}_k^o = h(\mathbf{x}_k) + \epsilon_k, \tag{2}$$

where ϵ_k is the observation error at time k. We use an ensemble of model simulations $\mathbf{X} = \{\mathbf{x}_{1,k}, \mathbf{x}_{2,k}, \ldots \mathbf{x}_{N_e-1,k}, \mathbf{x}_{N_e,k}\}$ to estimate the model state at each time. The mean of $\mathbf{X}$ before data assimilation (the background mean) is $\mathbf{x}_k^b$, and the ensemble mean after assimilation (the analysis mean) is $\mathbf{x}_k^a$. Likewise, the background error covariance matrix associated with the ensemble is $\mathbf{B}_k$. Ensemble model states can be projected into observation space with the forward operator h:

$$\mathbf{Z} = \{\mathbf{z}_{1,k}, \mathbf{z}_{2,k}, \ldots \mathbf{z}_{N_e-1,k}, \mathbf{z}_{N_e,k}\} \tag{3}$$

$$\mathbf{z}_{i,k} = h(\mathbf{x}_{i,k}), \quad 1 \le i \le N_e. \tag{4}$$

Note that $\mathbf{y}^o$ is used when dealing with real observations whereas $\mathbf{z}$ will be used to denote model state variables projected into observation space. We can also consider the ensemble means and background error covariance matrix in observation space:

$$\mathbf{z}_k^b = \mathbb{E}(\mathbf{z}_k | \mathbf{Y}_{k-1}^o), \tag{5}$$

$$\mathbf{z}_k^a = \mathbb{E}(\mathbf{z}_k | \mathbf{Y}_k^o), \tag{6}$$

$$\mathbf{B}_k^z = \mathrm{cov}(\mathbf{z}_k|\mathbf{Y}_{k-1}^o). \tag{7}$$

Next, we define the background and analysis innovations, as well as the analysis increment:

$$\mathbf{d}_{b,k}^o = \mathbf{y}_k^o - \mathbf{z}_k^b, \tag{8}$$

$$\mathbf{d}_{a,k}^o = \mathbf{y}_k^o - \mathbf{z}_k^a, \tag{9}$$

$$\mathbf{d}_{b,k}^a = \mathbf{z}_k^a - \mathbf{z}_k^b, \tag{10}$$

which describe the departures of model states from observations. The covariance matrix for $\mathbf{d}_{b,k}^o$ is called $\mathbf{S}_k$ (that is, $\mathbf{S}_k = \mathrm{cov}\left(\mathbf{d}_{b,k}^o|\mathbf{Y}_{k-1}^o\right)$). D05 show that, if the covariance matrices $\mathbf{R}$ and $\mathbf{H}\mathbf{B}_k\mathbf{H}^T$ are correctly specified, then

$$\mathbb{E}(\mathbf{d}_{b,k}^o(\mathbf{d}_{b,k}^o)^T) = \mathbf{S}_k \tag{11}$$

where again $\mathbf{H}$ is the tangent linear operator for h.

For the experiments presented in this paper, we impose that all observation errors are independent and identically distributed, so that estimation of $\mathbf{R}$ amounts to estimating a single observation error variance r. Similarly, we will use s and b^z to represent scalar versions of $\mathbf{S}$ and $\mathbf{B}^\mathbf{z}$ for single observations. All experiments use the National Center for Atmospheric Research (NCAR) Data Assimilation Research Testbed (UCAR/NSF NCAR/CISL/DAReS 2024). DART is a data assimilation software framework that supports multiple data assimilation methods for a range of idealized and real models. In particular, data assimilation is done using the Ensemble Adjustment Kalman Filter (EAKF; Anderson 2001) implemented via the parallel filtering algorithm described in Anderson and Collins (2007).

3. Methodology

We examine three different methods for estimating the scalar observation error variance r. Each method relies primarily on statistics generated during ensemble data assimilation to adaptively estimate r. For simplicity, we drop the time index k from all further equations and illustrate how each method functions at a single time.

a. The Desroziers Diagnostic

D05 shows that the relationship

$$\mathbb{E}(\mathbf{d}_b^o(\mathbf{d}_a^o)^T) = \mathbf{R} \tag{12}$$

holds if the matrix

$$\mathbf{HK} = \mathbf{HBH}^T\left(\mathbf{HBH}^T + \mathbf{R}\right) \tag{13}$$

agrees with the true background and observation error covariances (that is, if the matrices $\mathbf{HBH}^T$ and $\mathbf{R}$ are well-specified). This diagnostic check is often recast as an iterative scheme, where a sample version of the above expectation is computed periodically or whenever new observations are assimilated. In particular, given $\mathbf{d}_b^o$ and $\mathbf{d}_a^o$, we form a new estimate r^D:

$$r^D = \frac{1}{p}\left(\mathbf{d}_b^o\right)^T \mathbf{d}_a^o, \tag{14}$$

where again p is the dimension of $\mathbf{d}_b^o$ (which can also be viewed as the number of scalar observations assimilated). To mitigate potential issues of sampling deficiency in computing r^D, we use the exponential smoothing procedure described in Miyoshi et al. (2013): whenever the next estimate $\tilde{r}_{k+1}^D$ is computed, we choose a smoothing parameter $0 \leq \kappa \leq 1$ and let

$$r_{k+1}^D = \kappa r_k^D + (1-\kappa)\tilde{r}_{k+1}^D. \tag{15}$$

The Desroziers scheme is the only one of the three estimation methods that requires analysis innovations; therefore, the most current r estimate is computed *after* data assimilation, and cannot be used until the next cycle. Finally, we note that D05 also provides expectation-based estimates of s and b^z:

$$s^D = \frac{1}{p}\left(\mathbf{d}_b^o\right)^T \mathbf{d}_b^o, \tag{16}$$

$$b^{z,D} = \frac{1}{p}\left(\mathbf{d}_b^o\right)^T \mathbf{d}_b^a. \tag{17}$$

From these equations, it is clear that we can write

$$r^D = s^D - b^{z,D}, \tag{18}$$

i.e. the Desroziers estimate of r is the Desroziers estimate of b^z subtracted from the Desroziers estimate of s.

The Desroziers method has been used frequently in real numerical weather prediction experiments to estimate both diagonal elements of $\mathbf{R}$ only and the full covariance matrix. It has frequently been used for the quantification of uncertainty in satellite radiance measurements. Notable examples include Bormann and Bauer (2010), who estimate the variance and spatial correlations of clear-sky radiance observations in a European Centre for Medium-Range Weather Forecasts (ECMWF) assimilation system, and Campbell et al. (2017), who estimate interchannel correlations as well as diagonal elements and explicitly note a positive impact on forecast outcomes as a result. The method has also been used for other types of real-world observations, including satellite precipitation data (Kotsuki et al. 2017) and radio occultation observations (Semane et al. 2022).

b. The Karspeck Method

K16 presents an estimator for the (scalar) observation error variance r from a collection of observations based on ensemble-generated statistics. Observations can be binned in space and time to capture spatial and temporal variations in r, but we limit ourselves to the case of computing a single value at each time for simplicity. The Karspeck estimate of r is

$$\begin{aligned} r^K &= \frac{1}{p}\left(\mathbf{d}_b^o\right)^T \mathbf{d}_b^o - \frac{N_e+1}{N_e}\frac{1}{p}\sum_{j=1}^{p}\frac{1}{N_e-1}\sum_{i=1}^{N_e}\left([\mathbf{z}_i]_j - [\mathbf{z}^b]_j\right)^2, && (19)\\ &= s^D - b^{z,K}, && (20)\end{aligned}$$

where $[\mathbf{z}]_j$ is the j^{th} element of the vector $\mathbf{z}$. The first term is exactly s^D, the Desroziers estimate of s. The second term $b^{z,K}$ is a sample estimate of b^z, but is distinct from the Desroziers estimate $b^{z,D}$. Therefore, the Karspeck method differs from the Desroziers method only in how it forms an estimate of the background error variance. Specifically, the Desroziers estimator bases its estimate of b^z on the size of analysis increments. This means that it is dependent on the previous iteration's r and b^z estimates, as those variances determine the weighting of the background compared to observations during data assimilation. The Karspeck estimator, on the other hand, forms its estimate based exclusively on the background ensemble. The result is that no prior estimate of r is required, and that the estimator can be computed prior to data assimilation and immediately used the next time observations are assimilated. K16 demonstrates that the Karspeck estimator converges to the true observation error variance under certain conditions, and derives the variance of the estimator for the case that the observation error is Gaussian. They also verify the estimator against previous error variance estimates for in situ temperature observations in a global ocean general circulation model.

Just as the Desroziers estimator can be iteratively updated as new observations are assimilated, the Karspeck estimator can be computed for each new batch of observations. Accordingly, we implement the same temporal smoothing as with the Desroziers method in forming consecutive estimates with it. Additionally, the Karspeck estimator is not guaranteed to be positive by construction; in cases where the ensemble spread is significantly larger than it should be, or when a small number of observations is available, the computed estimate can be negative due to sampling deficiency. Whenever this occurs during data assimilation, we use the most recent Karspeck estimate instead to maintain consistency of the data assimilation system. In the majority of experiments, this only occurs once, before the very first assimilation window, when the ensemble spread is determined entirely by the prescribed initial conditions. We note exceptions to this behavior as they occur in the results section.

c. An Approximate Bayesian Inverse-Gamma Scheme

We present an approximate Bayesian scheme for modeling r. This scheme is numerically similar to the adaptive inflation strategy presented in Gharamti (2018) (hereafter E18), but with different input data and a modified strategy for updating the Bayesian parameter estimate. First, let r_0 be an initially assumed value of r. We seek to model a parameter ρ that acts to multiplicatively inflate r_0. As this parameter is updated, we obtain new estimates of r to use for data assimilation. As in E18, we use an inverse-gamma prior for ρ:

$$p(\rho) = \frac{\beta^{\alpha}}{\Gamma(\alpha)} \rho^{-\alpha-1} \exp(-\frac{\beta}{\rho}), \tag{21}$$

where α is a shape parameter that controls the tailedness and skew of the distribution and β is a scale parameter that controls its spread. Inverse-gamma distributions have been used previously for modeling variance parameters because they do not assign any probability to negative values and they assign very little probability to very small values (SB07). Rather than dealing with the inverse-gamma parameters α and β directly, we assume that a Gaussian mean and variance are initially specified, and then identify values of α and β to match the Gaussian parameters. This procedure is identical to the one described in Section 3b of E18.

When new observations are ingested, they are used sequentially to update the distribution for ρ. The likelihood of ρ given a new scalar observation (and corresponding background innovation) is given by

$$p(y^o | d_b^o) = \frac{1}{\sqrt{2\pi}\theta} \exp\left(-\frac{(d_b^o)^2}{2\theta^2} \right), \tag{22}$$

where $\theta^2 = b^z + \rho r_0$ is the innovation variance assuming the observation error variance ρr_0. Using the above prior with this likelihood, the posterior distribution $p(\rho | d_b^o)$ is

$$p(\rho | d_b^o) = \frac{\beta^{\alpha} \rho^{-\alpha-1}}{\sqrt{2\pi}\theta\Gamma(\alpha)} \exp\left(\frac{(d_b^o)^2}{2\theta^2} - \frac{\beta}{\rho} \right). \tag{23}$$

We set the next value of ρ to be the mode of the above posterior. To find the mode, we follow Anderson (2009) and E18 and do a first-order Taylor expansion of the likelihood about the prior mode ρ_b:

$$p(d_b^o | \rho) \cong \underbrace{p(d_b^o | \rho_b)}_{\bar{\ell}} + \underbrace{\left.\frac{\partial p(d_b^o | \rho)}{\partial \rho}\right|_{\rho_b}}_{\ell'} (\rho - \rho_b) + O(\rho - \rho_b)^2. \tag{24}$$

After multiplying this likelihood approximation with the Inverse-Gamma prior in (21) and taking a derivative with respect to ρ, we arrive at the quadratic equation

$$\left(1-\frac{\rho_b}{\beta}\right)\rho^2+\left(\frac{\bar{\ell}}{\ell'}-2\rho_b\right)\rho+\left(\rho_b^2-\frac{\bar{\ell}}{\ell'}\rho_b\right)=0. \tag{25}$$

Equations (24) and (25) are equivalent to equations (37) and (38) of E18, replacing their background covariance inflation parameter λ with the observation error variance inflation ρ. The difference from the E18 method is the use of the new likelihood (22). Equation (25) is then solved for ρ, and the real root closest to ρ_b is selected as the next inflation value. This value is multiplied with ρ_0 to yield the next estimate r^B of r. Finally, note that the posterior (23) is not exactly an inverse-gamma distribution, but it qualitatively retains many of the attractive properties of inverse-gamma distributions mentioned above. Accordingly, we identify new values for the parameters α and β and refit the distribution to an inverse-gamma one as in E18. In doing so, we have established a scheme that can be cycled continuously as new batches of observations are ingested. Although this approach generates a new estimate r^B with every scalar observation, we allow all observations from a given assimilation period to update the estimate before it is next used, so that we only have one single r estimate per assimilation period as with the previous two methods.

This approximate Bayesian inverse-gamma scheme is similar to the Bayesian Adaptive Ensemble Kalman Filter approach described by Stroud et al. (2018), but with a different handling of the marginal posterior for estimated parameters. We note one potential shortcoming of this scheme: the variance of an inverse gamma distribution is inversely proportional to α^3, and the mean/mode of an inverse gamma distribution are proportional to $\frac{\beta}{\alpha}$. As a result, if the variance of the posterior distribution shrinks over the course of ingesting many observations, α and β may dramatically increase. Because the process of refitting the posterior to an inverse gamma distribution requires evaluating the PDF of the distribution, this eventually leads to dealing with values near the upper bound of double precision, resulting in computational challenges associated with rounding errors and indeterminate forms. When this occurs, we opt to revert the variance of the new inverse gamma distribution to the variance from the previous iteration. Although the scheme allows for the variance of the distribution to increase or decrease (E18), this essentially imposes a lower bound on the variance of the distributional estimate. We find empirically that this lower bound usually lies between approximately 0.0001 and 0.01. Additionally, once this lower bound is encountered, it is difficult for the variance to increase significantly again. We note that this numerical issue can theoretically manifest in errors for the E18 spatially-varying adaptive inflation scheme. However, appropriate values for individual spatially-varying inflation coefficients are likely to evolve much faster than a single spatially averaged r estimate, reducing the chance of encountering small posterior inverse-gamma variances. It is possible to manually impose a lower bound on the estimator variance; for the purposes of estimating a spatially-averaged, time-invariant r, however, it would be preferable to allow the variance to shrink as much as it should without such heuristics. We set our minimum variance threshold to 0.0001 for all experiments in this study. A brief analysis of the evolution of the variance of the Bayesian estimator is given in appendix A1.

4. Model Experiments

We explore the behavior of each method using 2 idealized dynamical models. The first is the Lorenz (1963) model, which is a 3-variable system (x_1, x_2, x_3) governed by the following system of ordinary differential equations:

$$\frac{\mathrm{d}x_1}{\mathrm{d}t} = \sigma(x_2 - x_1), \tag{26}$$
$$\frac{\mathrm{d}x_2}{\mathrm{d}t} = x_1(\rho - x_3) - x_2, \tag{27}$$
$$\frac{\mathrm{d}x_3}{\mathrm{d}t} = x_1 x_2 - \beta x_3. \tag{28}$$

The parameters σ, ρ, and β are unrelated to any of the variables described in section 3; we set them to the standard values of 10, 28, and $\frac{8}{3}$ for all experiments in this study. For this model, we use an 80-member ensemble and a non-dimensional time step of 0.001. We assimilate observations of the entire state (i.e. all three state variables) every 30 time steps for a total of 10000 assimilation periods.

The second model is Model III from Lorenz (2005), a 960-variable system composed of a small scale and a large scale that interact with each other and project onto a single variable. Specifically, the model is governed by the following ordinary differential equation at the n^{th} grid point:

$$\frac{\mathrm{d}Z_n}{\mathrm{d}t} = [X,X]_{K,n} + b^2[Y,Y]_{1,n} + c[Y,X]_{1,n} - X_n - bY_n + F, \tag{29}$$

where X and Y represent the large and small scale contributions to the state Z, respectively, c is a coupling parameter, b controls the amplitude and frequency of the small-scale waves, F represents an external forcing, and K controls the wavenumber of the large-scale waves. Expressions of the form $[X,Y]_{a,n}$, etc. represent a sum of products of values of X and Y surrounding the n^{th} grid point that introduces spatial correlations between nearby grid points, where a essentially is a length scale. We use a 500-member ensemble with the same non-dimensional time step, and assimilate observations located at every other grid point (i.e. 480 observations) every 30 time steps. Experiments with Model III are integrated forward for a total of 2000 assimilation periods.

Unless otherwise stated, all experiments use the identity operator as the forward operator. We expect that some differences in the performance of the three estimation methods from one model to the other will result from the number of observations available during each assimilation period to form an estimate. For the L63 model, only 3 observations are available at each time compared to 480 for the 2005 model, so the risk of sampling deficiency is greater. Accordingly, we present the results of each experiment for both models together. We use a slightly stronger temporal smoothing parameter ($\kappa = 0.005$) for the L63 experiments than for the L05 experiments ($\kappa = 0.01$). For the ABIG scheme, the initial distribution for ρ is chosen to have mean equal to 1. We set the initial standard deviation of the ρ distribution to 0.25 for the L63 experiments and to 0.5 for the L05 experiments.

5. Results

For each set of experiments, we begin with the assumption that observation errors are Gaussian with mean 0 and variance 2. We record the r estimates generated by each method over the course of each simulation. For the Desroziers and Karspeck methods, we also plot the b^z estimates used in each estimate (see Eqs. 16 and 19). Figures 1 and 2 show root mean square errors (RMSE) for each experiment (values), as well as changes in RMSE relative to a run where no r estimation is performed (shading). From this point forward, and in the following figures, we will adopt the following shorthand descriptions of each method when presenting findings: the Desroziers estimator will be called DRZ; the Karspeck method will be called KAR; the approximate Bayesian inverse-gamma method will be called ABIG; experiments where no estimation of r is performed will be called NONE.

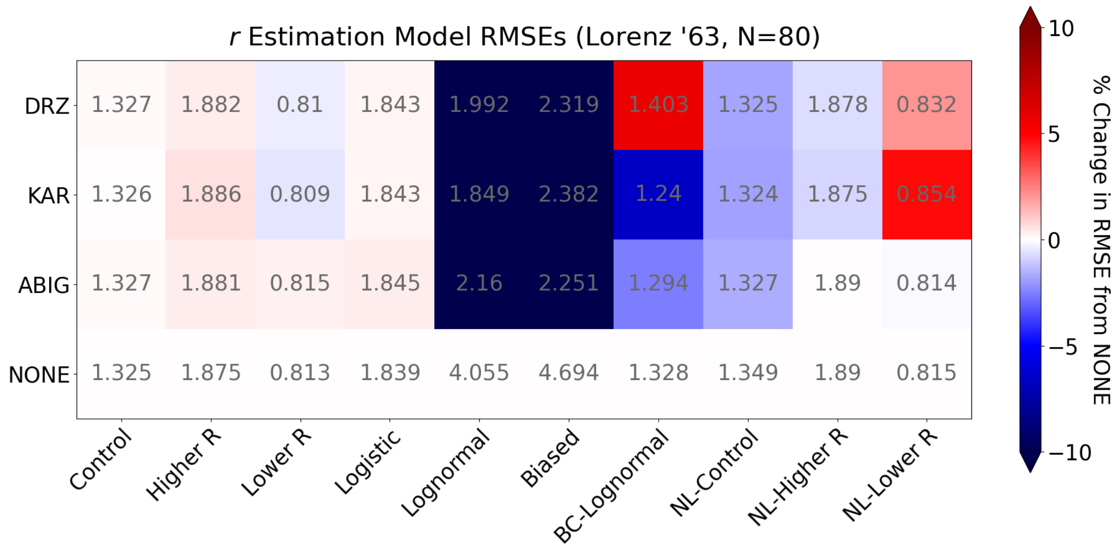

FIG. 1: Observation space root mean square errors (RMSEs) for each r estimation experiment with the L63 model. Shading indicates a percent change in RMSE relative to experiments where no r estimation was performed.

a. Control Experiment

First, we examine the case where the initially specified variance is actually correct, so that each method only needs to maintain the correct value. Figures 3 and 4 show the estimates generated during these control experiments. In the L63 experiments, all three methods track the true r value (=2) with approximately the same skill. In the L05 experiments, where the sample size is larger, the DRZ and KAR methods generate estimates that are much smoother in time than the L63 experiments. This does not happen with the ABIG method; the ABIG estimate briefly drops in the first couple assimilation cycles but then quickly centers on the correct value. However, the variance of the estimate reaches its minimum permissible value and so the noise in the ABIG estimate does not drop as much as with the other two methods.

We also observe that, in both experiments, the DRZ estimate of b^z is significantly noisier than the KAR estimate, although both are centered on the same value. This is especially true for the L63 experiments, for which the innovations at each assimilation cycle are much larger. This is

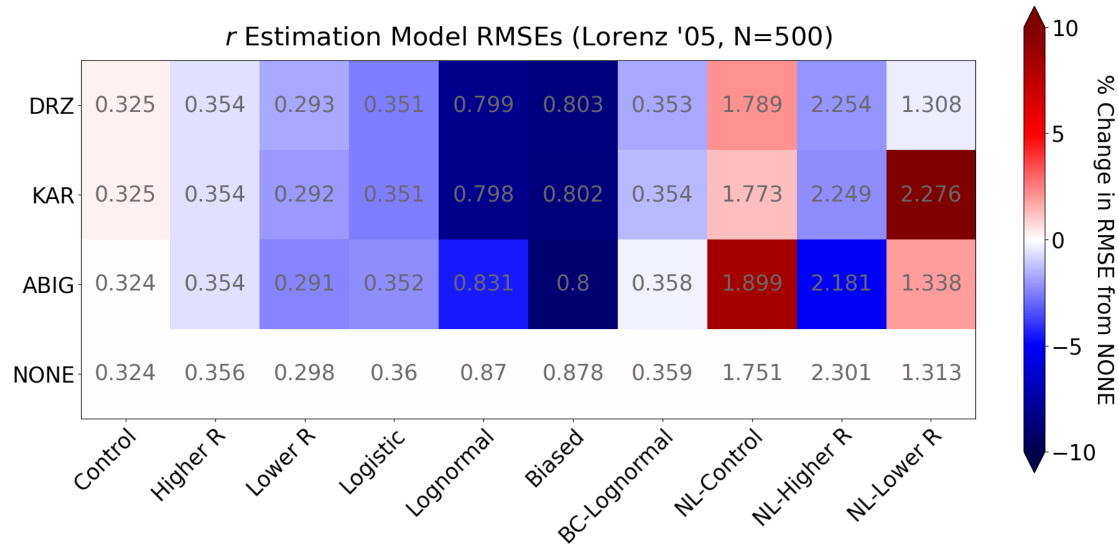

FIG. 2: As in Figure 1, but for the L05 experiments.

expected behavior; the Desroziers estimate of b^z is directly proportional to $\mathbf{d}_b^o$ (see Equation 16), which can vary much more than the background ensemble variance that determines the KAR estimate (Equation 19). Because of the temporal smoothing applied to both estimates, however, this difference has very little impact on the resulting r estimates. Note that in offline experiments performed without any temporal smoothing, estimates of r varied significantly over short time frames, resulting in significantly worse analyses and forecasts. This is especially true for the L63 model, where only 3 observations are used for each estimate. For all experiments in this group, there is minimal impact on forecast RMSE, because the r values used during data assimilation are very close to the (correct) control value.

b. Gaussian Errors with Misspecified Variances

The next set of experiments uses observations with Gaussian errors, but with a different variance than is initially assumed. In particular, we still start each experiment assuming $r = 2$, but we consider both the case when the true observation error variance is underestimated ($r = 4$; Figures 5 and 6) and the case when it is overestimated ($r = 0.75$; Figures 7 and 8). In these experiments, all three methods again center on the correct r value after some initial spin-up time. Many of the same differences in the estimators' performance persist from the previous experiments; notably, the increased noise in the DRZ estimate of b^z and the lower bound on the ABIG estimator's variance. We also note that in the L05 experiments, and for all L05 experiments where ABIG does converge to the correct r, it does so much more rapidly than the DRZ and KAR methods. This may be due to the sequential nature of the ABIG algorithm compared to the intermittent averaging approach of the other two methods. Estimating r leads to some improvement in forecast outcomes when the initially prescribed variance is incorrect. These improvements are only on the order of a 1-2% reduction in RMSE, and are especially marginal for the L63 model, suggesting that the background uncertainty dominates the uncertainty in the analysis in those model experiments.

c. Symmetric, Unbiased, Non-Gaussian Errors

The previous experiments focus on the case of Gaussian observation errors; we now examine how well these methods are able to recover the correct variance of the observation error even if the observation error has non-zero higher moments. A simple first test is the logistic distribution, which is still symmetric but with more probability density focused near the tails and the center of the distribution than a Gaussian. We use a logistic distribution with mean $\mu = 0$ and true variance $r = 4$. The results of these experiments (Figures 9 and 10) are very similar to the previous experiments with an underestimated Gaussian variance. For both models, all three methods converge to the correct r, with the same noted caveats about the variance in each estimator. However, we see a greater reduction in RMSE from performing r estimation in these experiments.

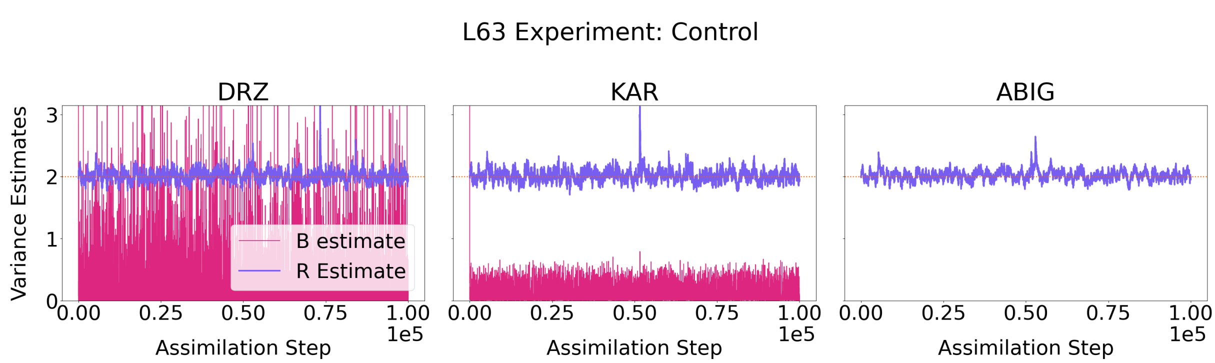

Fig. 3: r estimates generated by each method during L63 experiments when errors are Gaussian with mean 0 and variance 2 (i.e. when they match the assumed distribution of observation errors). Magenta curves represent the b^z estimates used by the DRZ and KAR methods.

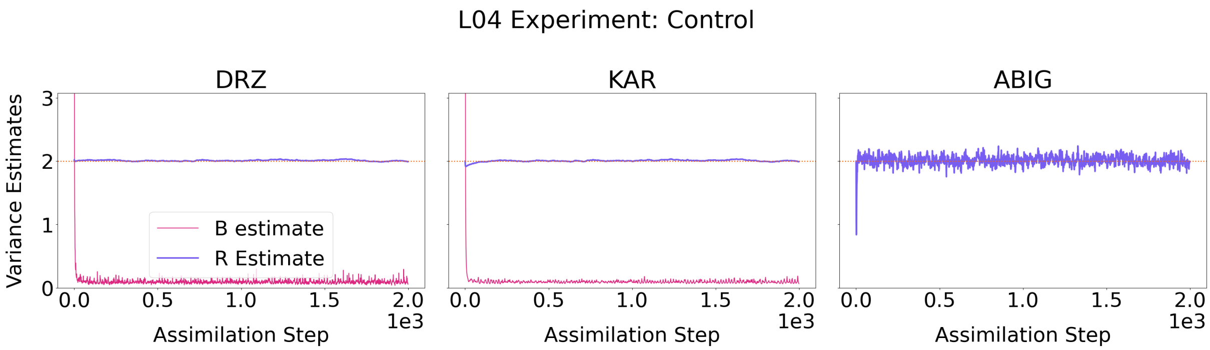

FIG. 4: As in Figure 3, but for L05 experiments.

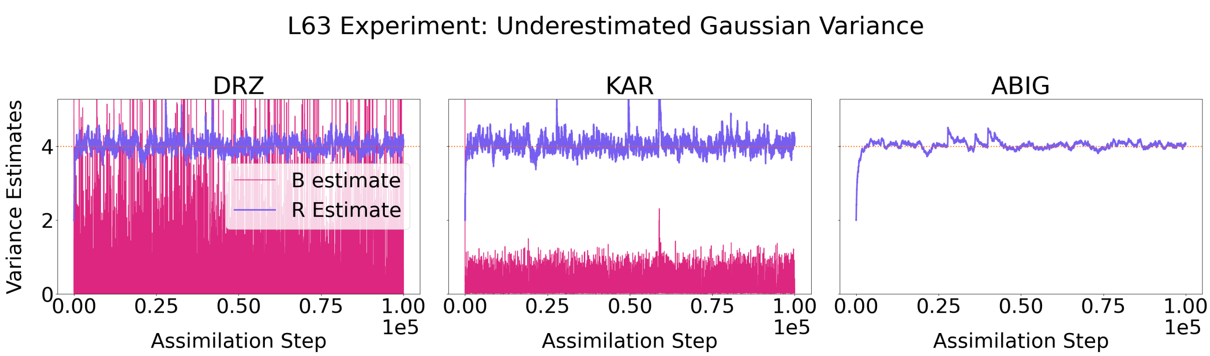

FIG. 5: r estimates generated by each method during L63 experiments when errors are Gaussian with mean 0 and variance 4.

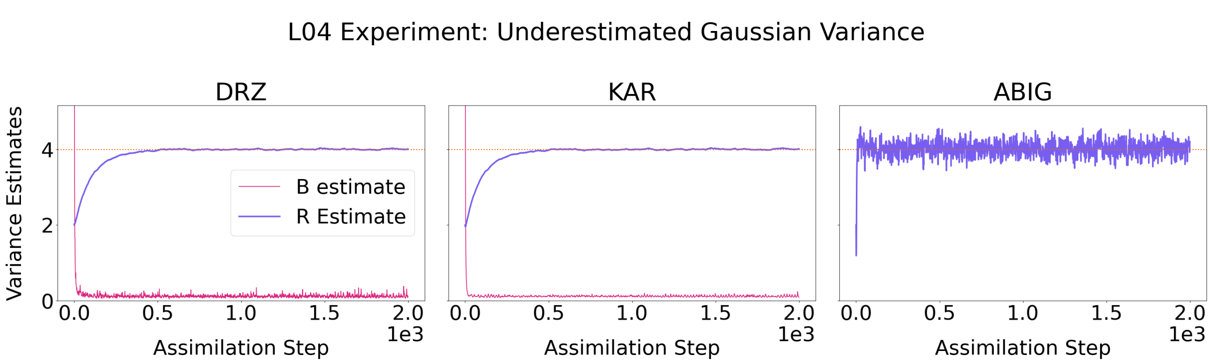

FIG. 6: As in Figure 5, but for L05 experiments.

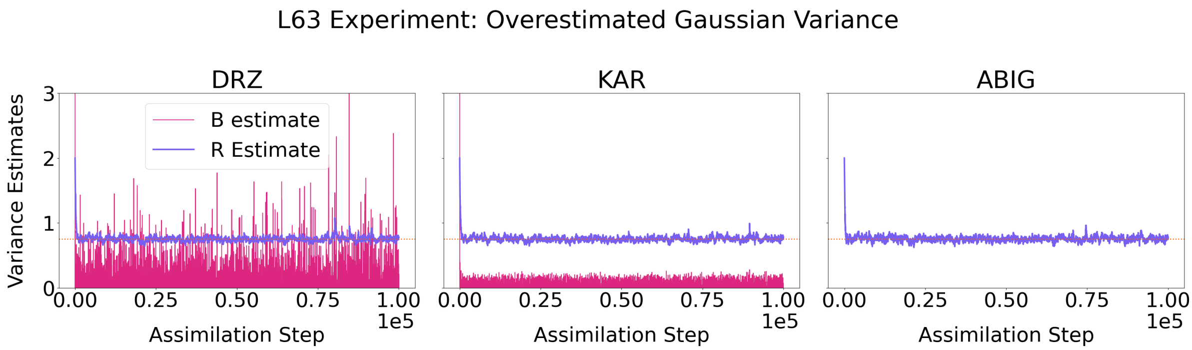

FIG. 7: r estimates generated by each method during L63 experiments when errors are Gaussian with mean 0 and variance 0.75.

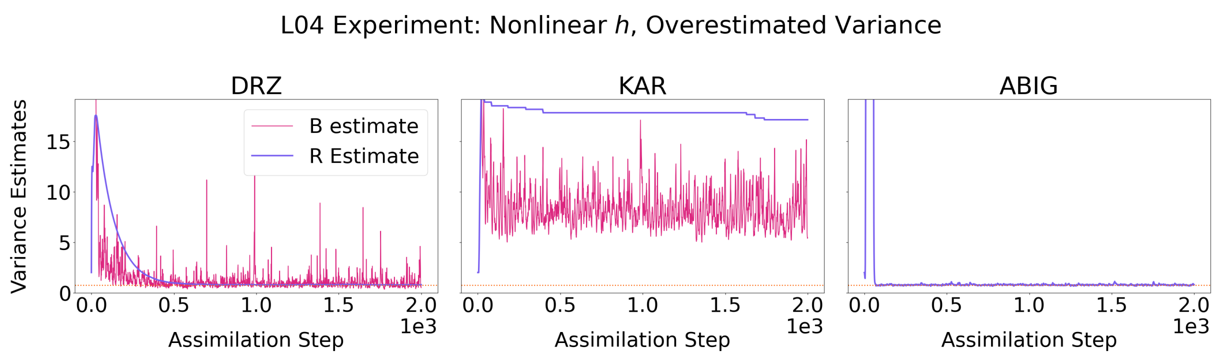

FIG. 8: As in Figure 7, but for L05 experiments.

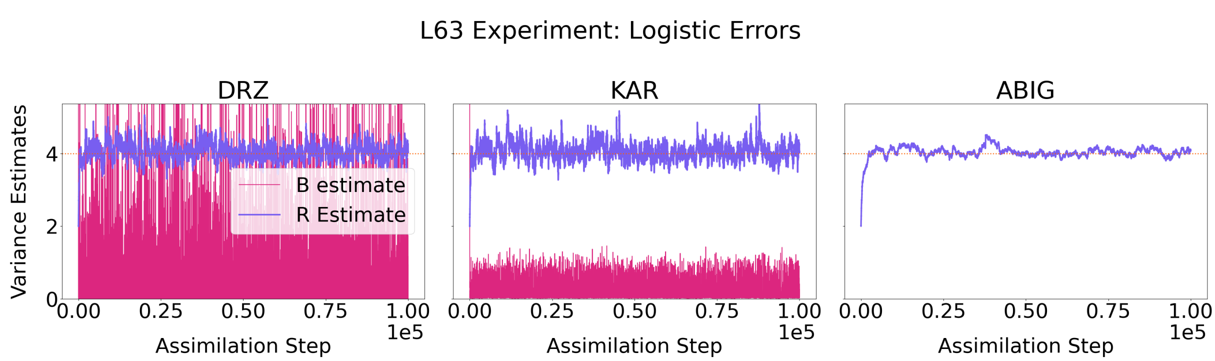

FIG. 9: r estimates generated by each method during L63 experiments when errors are Logistic with mean 0 and variance 4.

d. Skewed, Biased, Non-Gaussian Errors

Many real-world observations have errors that are not well-modeled by symmetric distributions with 0 mean. Specifically, variables that are bounded below (e.g. precipitation, tracer concen-

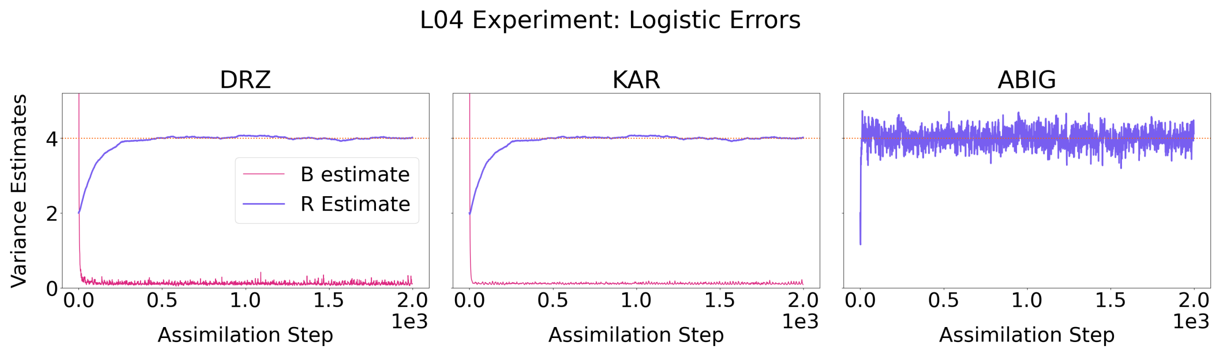

FIG. 10: As in Figure 9, but for L05 experiments.

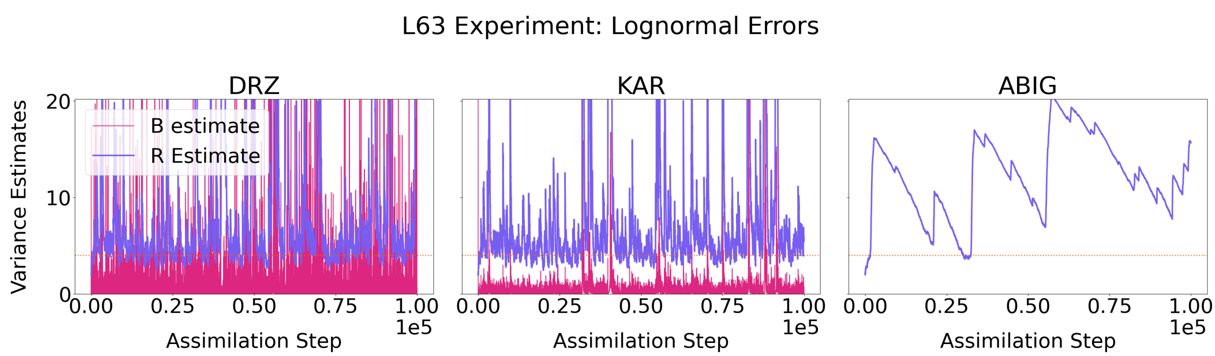

FIG. 11: r estimates generated by each method during L63 experiments when errors are Log-normal with mean 1 and variance 4.

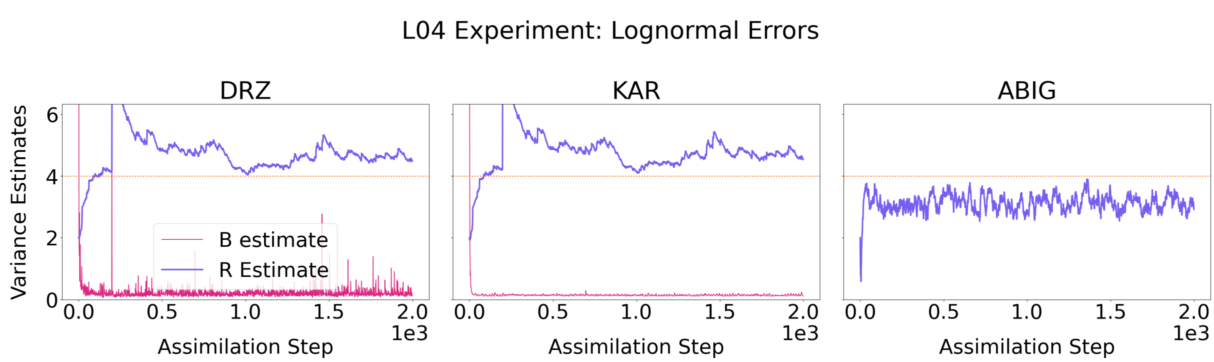

FIG. 12: As in Figure 11, but for L05 experiments.

tration, sea ice thickness) can never take on negative values, so attempting to assimilate them assuming Gaussian errors can lead to nonphysical results - especially when the observed values themselves are very small. With that in mind, we now consider how well r can be estimated when the observation error is distributed log-normally (i.e. bounded below and skewed to the right). If

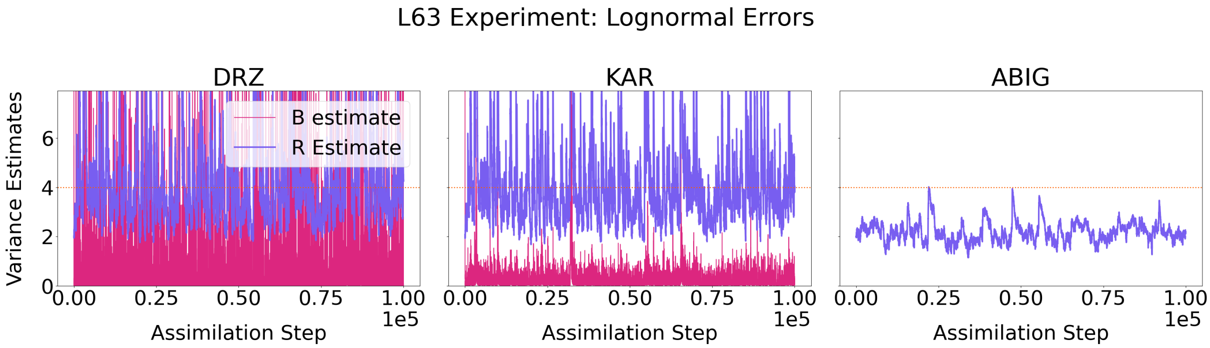

FIG. 13: r estimates generated by each method during L63 experiments when errors are Log-normal with mean 0 and variance 4.

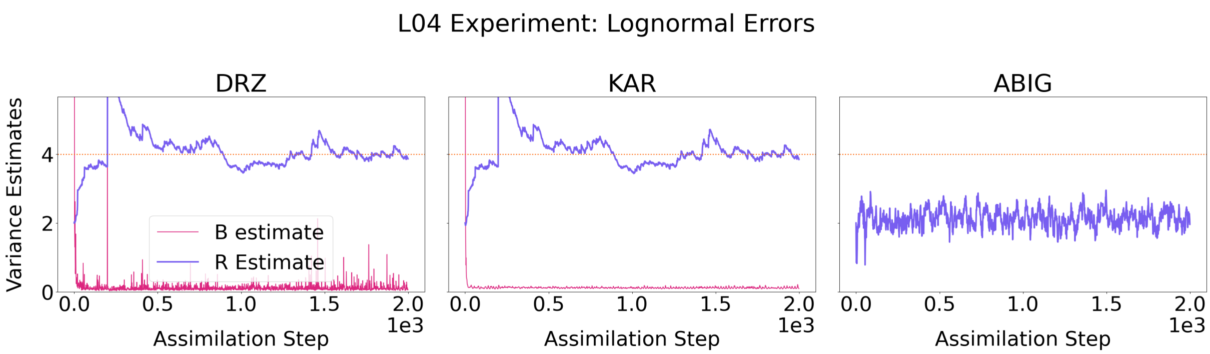

FIG. 14: As in Figure 13, but for L05 experiments.

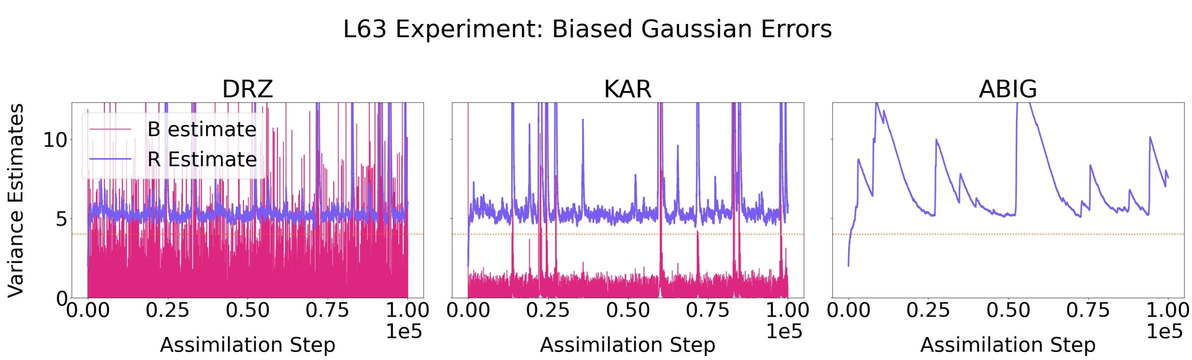

FIG. 15: r estimates generated by each method during L63 experiments when errors are Gaussian with mean 1 and variance 4.

the second moment of such non-Gaussian distributions can be recovered, it can be used both when Gaussian assumptions are still incorrectly imposed and, when using data assimilation strategies

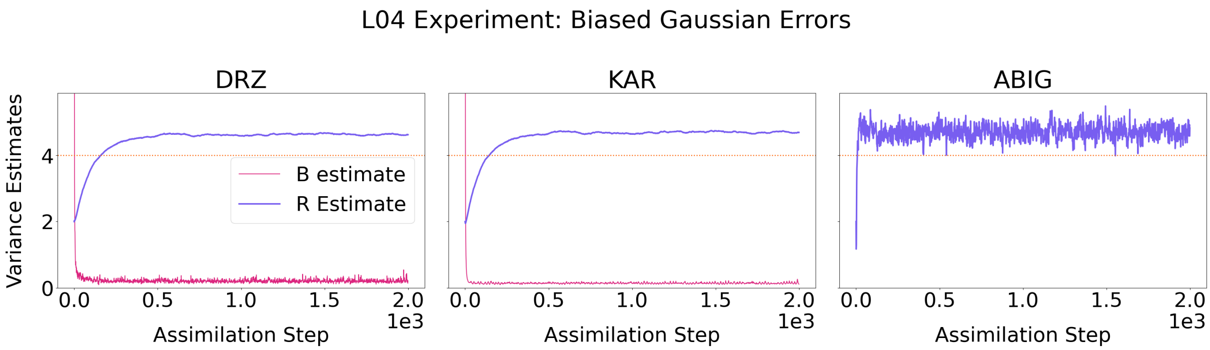

FIG. 16: As in Figure 15, but for L05 experiments.

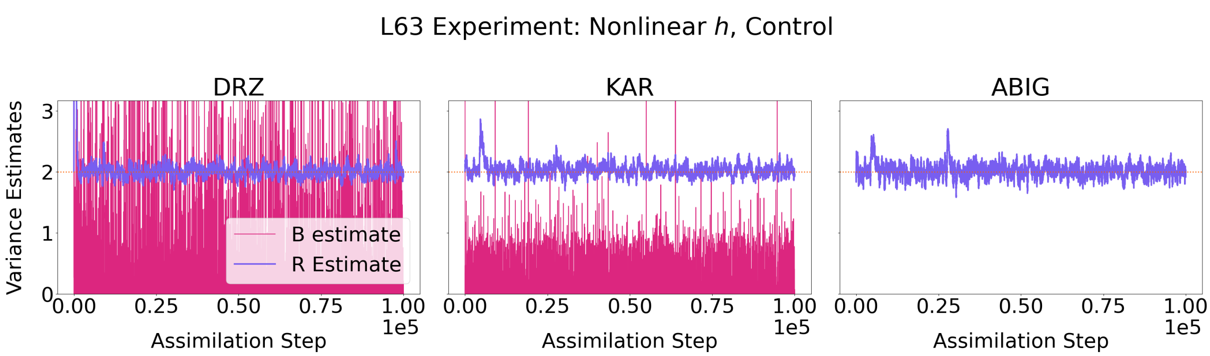

FIG. 17: r estimates generated by each method during L63 experiments when errors are Gaussian with mean 0 and variance 2, and observations are made using a quadratic forward operator.

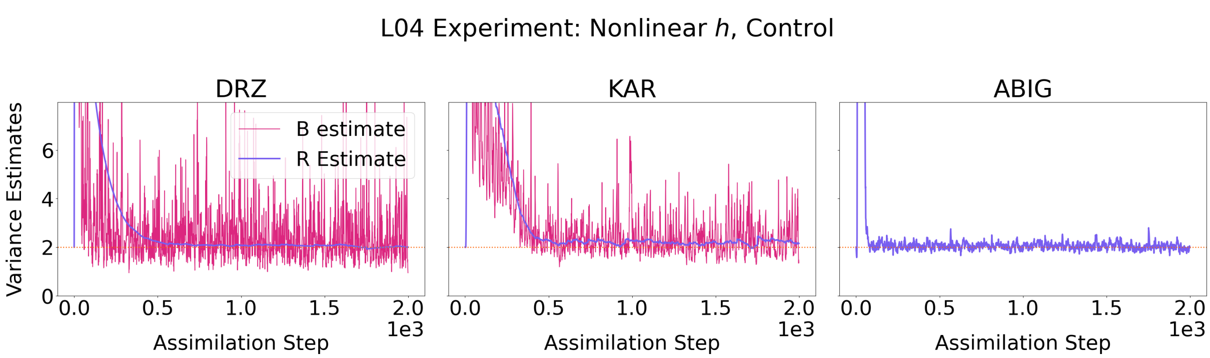

FIG. 18: As in Figure 17, but for L05 experiments.

that allow for non-Gaussian likelihoods, to inform the selection of a suitable likelihood with an appropriate spread.

Figures 11 and 12 show the results of the experiments with log-normal errors. The chosen log-normal distribution has mean equal to 1 and variance equal to 4. All three methods fail to stably

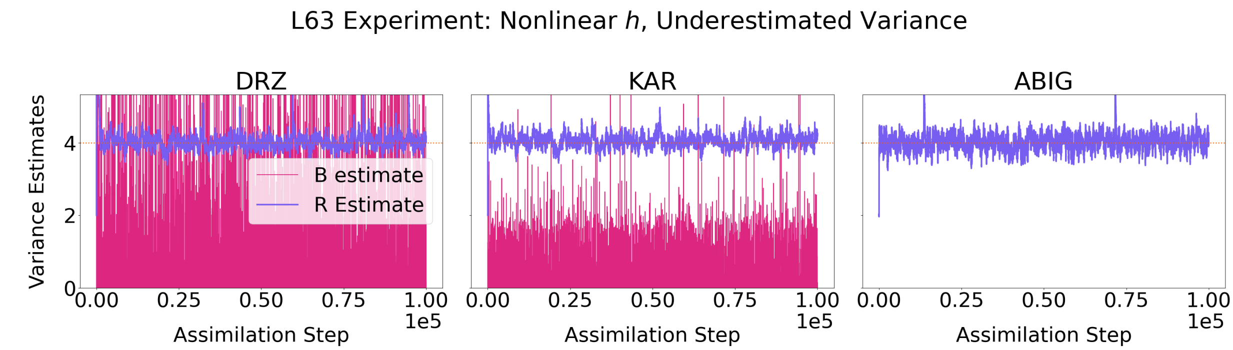

FIG. 19: r estimates generated by each method during L63 experiments when errors are Gaussian with mean 0 and variance 4, and observations are made using a quadratic forward operator.

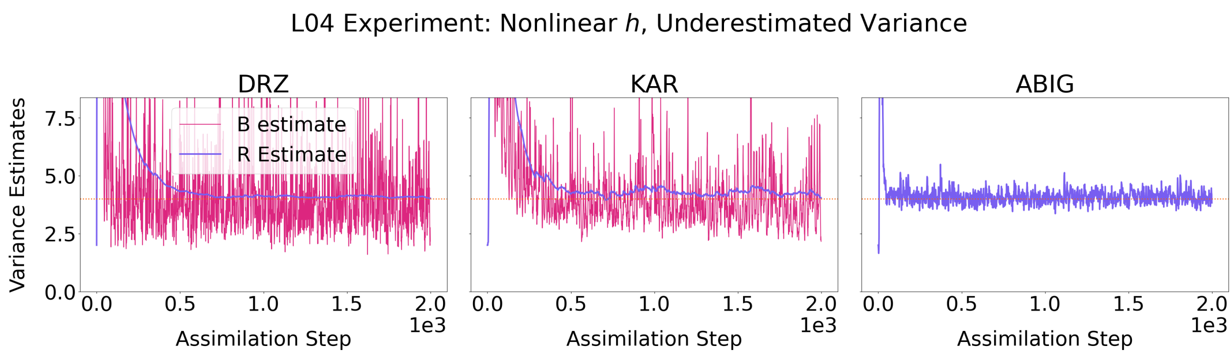

FIG. 20: As in Figure 19, but for L05 experiments.

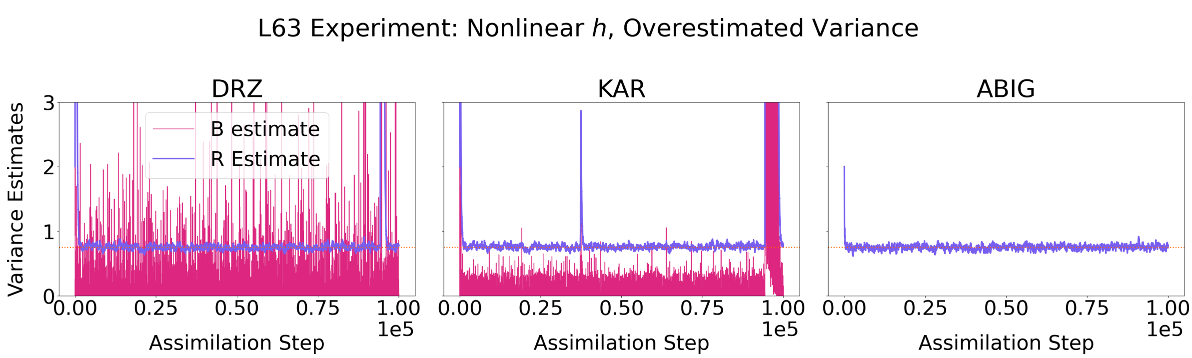

FIG. 21: r estimates generated by each method during L63 experiments when errors are Gaussian with mean 0 and variance 0.75, and observations are made using a quadratic forward operator.

converge to a single r estimate. In the L63 experiments, the Desroziers and Karspeck estimators both consistently overestimate the correct variance slightly, and sometimes rise dramatically when innovations grow very large. This occurs whenever the observation error is an extreme value from

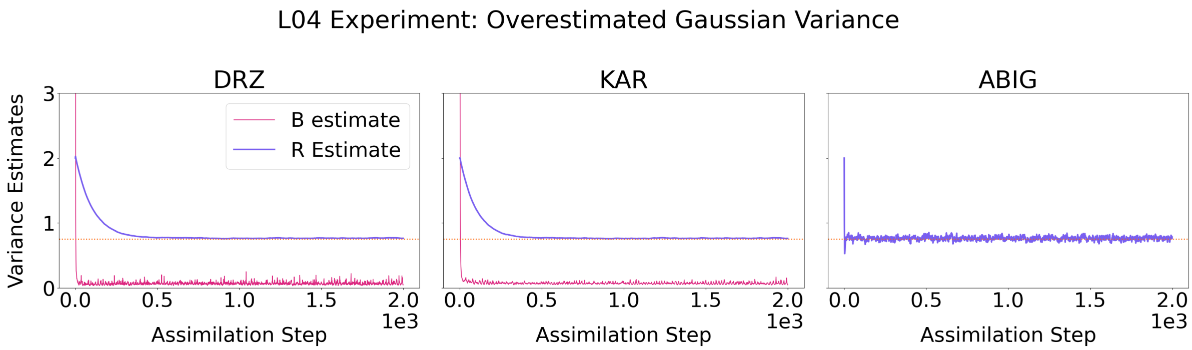

FIG. 22: As in Figure 21, but for L05 experiments.

the positive tail of the log-normal distribution. The ABIG estimator also increases sporadically; however, it does so less frequently than the other two, but takes longer to return to values close to the true variance. Despite the issues associated with each method, each method generally increases r and leads to a 50% reduction in RMSE compared to when no estimation is performed. In the L05 experiments, when a much larger volume of observations is available per estimate, the spikes in DRZ and KAR are largely mitigated, although the estimates still have a positive bias and behave erratically at times. Interestingly, the approximate Bayesian scheme stays close to the initially prescribed incorrect r, increasing slightly from that value but still underestimating the correct value. This may occur because enough samples from the main body of the log-normal distribution are ingested for the Bayesian scheme to grow very confident in an estimate before more extreme observation errors are considered. While we see improvements in RMSE from all methods, the improvement is accordingly more substantial with DRZ and KAR than with ABIG.

Assimilating observations with log-normal errors poses two distinct challenges; the resulting observations will 1) always be biased and 2) occasionally take on extreme positive values. We next examine each of these issues in isolation to identify which aspects of this section's results arise from which issue.

e. Skewed, Unbiased, Non-Gaussian Errors

Figures 13 and 14 show r estimates generated when the log-normal errors are shifted to have mean equal to 0. In the L63 experiments, doing so reduces the magnitude of the sudden increases noted for the DRZ and KAR methods, though neither centers the estimates on the correct r value (the average DRZ estimate over the course of this experiment is 6.76; the average KAR estimate is 4.76). The erratic behavior in the ABIG estimator is also eliminated, but it does not move away from the initially prescribed incorrect r significantly. The DRZ estimator in this experiment is the only one to notably worsen forecast outcomes, increasing RMSE by about 6% relative to doing no estimation. The difference in performance of the DRZ estimator, when relatively few samples are available, may be due to the fact that the DRZ estimator is the only one that uses analysis statistics to form its estimate. If the updates performed following several sequential data assimilation steps are negatively impacted by ignoring higher-order moments, it is possible that the resulting r^D can be adversely affected.

With the bias removed from log-normally distributed observation errors, the bias in both the DRZ and KAR estimators also disappears in the L05 experiments (Figure 14). This convergence occurs following an initial spike at around 250 assimilation steps. The ABIG estimator also decreases when the bias is removed; however, because the ABIG estimate in the log-normal error regime was too small to begin with, the resulting estimate here is even further from the correct value. The average estimate over the experiment is 1.91. Improvements in RMSEs are smaller in these experiments than with the full biased log-normal errors, and disappear completely for the ABIG experiment. Note, however, that the absolute RMSE values themselves are also considerably lower when the bias in observation errors is removed.

f. Biased Gaussian Errors

Figures 15 and 16 show r estimates generated when observation errors are Gaussian but with a positive bias. Here, the observation error is Gaussian with mean equal to 1 and variance 4. For the L63 model, this bias leads to positive bias and sporadic increases in all three estimators similar to the log-normal experiments, although not quite as extreme. Once again, the DRZ and KAR methods briefly reach much larger values before returning immediately to an approximately constant baseline. The ABIG estimator behaves similarly in this case. All three methods yield similar reductions in RMSE to each other and to the log-normal experiments with the L63 model. The ABIG estimator yielded slightly better performance relative to the other two methods than in the log-normal experiment.

Ingesting and assimilating biased observations in the L05 model leads to very stable, but still biased, r estimates (Figure 16). These estimates are smooth in time for the DRZ and KAR methods; for the ABIG method, we once again see that some amount of noise in r^A persists with time despite the lack of significant changes over time. However, all three estimates remain near the same value (approximately 4.5) after some initial spin up. All three methods see a similar reduction in RMSE despite their differences.

g. Nonlinear Forward Operators

Finally, we briefly consider the problem of estimating r when the forward operator h is nonlinear. We perform the following experiments assimilating the square of the state (i.e. $h(x) = x^2$). We only show results for observation errors that are Gaussian distributed. For the L05 model, we also performed further tuning of the localization radius, which amounted to a reduced radius to prevent spuriously large sub-optimal updates from spreading to nearby state variables. Figures 17, 19, and 21 show estimates generated during L63 experiments when r is initially assumed to be 2 and the true r is 2, 4 and 0.75, respectively. We note that, for all experiments with a nonlinear h, the KAR method yielded negative r estimates much more frequently than in all previous experiments (1005, 1789, and 1610 times out of 100000, respectively). Figures 18, 20, and 22 show the corresponding experiments for the L05 model (the KAR method was negative in these experiments (178, 26, and 1957 times out of 2000, respectively). When the initially assumed r is correct (Figures 17 and 18), it is still possible to recover the correct r with each method. Although the ABIG estimator is able to recover the correct r faster than the other two methods in the L05 experiment, it retains the most noise as in the linear h case. The KAR estimator also maintains a slight positive bias in both of these experiments, particularly for the Lorenz '04 model, though this does not lead to a significant degradation in forecast RMSE.

The most consistent improvements in forecast outcomes arise when the initially assumed r is an underestimate of the true observation error variance (Figures 19 and 20). Much of the same behavior is present from the previous experiments, namely the positive bias in the KAR estimate and the differences in noise present in the ABIG estimate. Estimating r from nonlinear observations when it is initially overestimated is a larger challenge. In the L63 experiments, all estimators perform fairly well up until after approximately 90000 assimilation cycles. At that time, the true state enters a regime where both the background innovations and the background error variance increase dramatically, leading to a corresponding increase in the DRZ and KAR estimators. The DRZ estimate recovers quickly to the correct r estimate. Meanwhile, the KAR estimate also recovers but takes much longer to do so. The ABIG estimate is the only one that does not deviate significantly from the correct value. As a result, the KAR experiment experiences a negative impact on forecast outcomes, and the ABIG experiment is the only one that does not adversely affect them. In the L05 experiments, both the DRZ and ABIG estimators recover the correct r, though only the DRZ method resulted in an improvement in forecast outcomes. The KAR estimator, however, increased significantly at the start of the experiment and then very frequently estimated negative values for r, leading to the previous estimate being used. The result is that the KAR estimator stayed very large for the entire experiment. The tendency for the Karspeck estimator to be negative in this experiment is likely a result of the initial rise in the background error variance during the start of the experiment, exacerbated by the overestimation of the variance and the quadratic forward operator. The first term on the right hand side of Equation (19) will be relatively small because observations have smaller errors, and any sufficiently large background errors will be increased further when transformed into observation space, resulting in the second term being relatively large. Although the filter did not diverge from the correct model state in this experiment, the large r estimate generated by the Karspeck method led to a near-doubling in forecast RMSE compared to the NONE experiment.

6. Discussion and Conclusions

We have constructed a new Bayesian algorithm for sequential estimation of a scalar observation error variance based on an inverse gamma prior and a modified Gaussian likelihood. Additionally, we have used two idealized models to compare this new method against the common Desroziers ”diagnostic check” scheme and the method of K16, another ensemble-based estimator. All methods effectively recover the correct observation error variance when the distribution of observation errors is unbiased and symmetric, even in the case of non-Gaussian distributions. When uncorrected bias is present in the observation error, numeric instabilities sporadically appear in all estimates of the variance, as well as a bias in the variance estimates themselves. This bias is usually positive and reduces the reliance of the assimilation system on the biased observations. Certainly, there are numerous existing methods for addressing bias in observations more directly that are preferable (e.g., Knisely and Poterjoy 2023; Chandramouli et al. 2022), but it is useful to note that these methods can continue to improve forecast outcomes even with bias present in observations. Finally, we demonstrate that these methods are sometimes able to function even when the forward operator relating the model state to observations is nonlinear, although their benefits are not as clear as for the linear case and some difficulties arise when the true observation error variance is relatively small. Based on these findings, it is reasonable to conclude that any of the three methods could benefit forecast quality in real-world applications where observation errors are known to be approximately unbiased and Gaussian. However, there is some evidence that estimating the variance in bounded observations with non-Gaussian errors, such as fractional sea ice concentration or gas concentrations, may be challenging. The same is true for observations where h is nonlinear, such as all-sky radiance or reflectivity observations.

Though the approximate Bayesian inverse-gamma scheme is generally effective at correctly estimating the true observation error variance, numerical issues place a lower bound on the amount of noise present in the estimator and can potentially limit its ability to evolve as new observations are ingested. The fundamental problem associated with these numerical issues is that the inverse-gamma PDF can grow very large as its variance shrinks. Moving forward, it might be prudent to continue designing methods that do not require direct evaluation of the inverse-gamma PDF (e.g., Stroud and Bengtsson 2007), or to leverage prior distributions with more suitable parameters. In general, whenever any Bayesian scheme is used to estimate parameters of the modeling or assimilation process, care should be taken in determining how the variance of the distributional estimate is allowed to evolve. A tendency toward priors with higher variances will allow new observations to more strongly affect the parameter estimate, whereas smaller variances will yield less noisy estimates that evolve slower and more smoothly in time.

We also note that only the Desroziers method has been previously implemented for estimating the full observation error covariance matrix R (i.e. accounting for correlated observation errors). In order to do the same for the Bayesian scheme, further parameterization of the full covariance matrix would be necessary, along with a method for updating the new parameters (e.g., Stroud et al. 2018). However, it is straightforward to extend the Karspeck ensemble estimator to account for off-diagonal elements in a similar manner to the Desroziers estimator. The Karspeck estimator frequently performed similar to or better than the other two estimators in terms of improving forecast outcomes, and has the added advantage that it can be used immediately for new observations as they are assimilated. Accordingly, it should be investigated further as an alternative to the Desroziers scheme for use with real-world, correlated observations.

Finally, we point out related research questions that are not encompassed by our study but remain interesting for the problem of approximating statistics of observation errors. Notably, we do not consider the possibility of state-dependent observation errors in this work at all. Some methods already exist to assimilate observations where the dependence on the state is already known (e.g., Bishop 2019, 2016); however, there is relatively little research dedicated to estimating the distribution of state dependent observation errors when the dependence itself is not a priori known. On a related note, we also make no attempt here to estimate the full PDF of non-Gaussian observation errors, even though we successfully retrieve the second moment of such distributions. Hu et al. (2024) present one method for doing so based on computing a deconvolution of the background error PDF from the background innovation PDF, but future research should continue to investigate other approaches.

APPENDIX

A1. Analysis of the ABIG Estimator Variance

Figures A1 and A3 show the evolution of the variance of the ABIG estimator's posterior distribution for ρ for all experiments where the true observation error is Gaussian, as well as for the log-normal experiment. In all of these cases, the posterior variance generally decreases until the inverse-gamma parameters grow large enough that evaluating their PDFs yields values outside of double precision. Whenever this happens, the previously estimated posterior variance is reused. This often occurs repeatedly throughout the remainder of the run, or sometimes indefinitely, resulting in a collapse to a single posterior variance. Because the parameters of an inverse-gamma distribution depend on the distribution's mean as well as its variance, the posterior variance that each experiment ends in the vicinity of varies with the ρ value that the ABIG estimator approaches over time (i.e. with the observation error variance that the ABIG estimator predicts). As a result, experiments where ABIG estimated higher r values usually correspond with larger final posterior variances, and vice versa. Finally, because of the sequential nature of the ABIG algorithm, note that much of the decrease in the posterior variance occurs rapidly, relatively early in each experiment. One consequence of this behavior is that raising the initial prior variance for the ABIG estimator had minimal effect on when or where the collapse of the posterior variance occurs. Figure ME NEXT shows the evolution of the posterior variance for the L05 experiments when the initially prescribed prior standard deviation increases from the value prescribed in all of the other experiments. Regardless of the initially prescribed standard deviation, the posterior variance shrinks to approximately 0.01 before evolving erratically for a period and then fixing to a single value. Note that the final posterior variance each of these experiments achieves is not necessarily consistent with which experiment started with the largest prior standard deviations, and that the best forecast RMSEs in these experiments occurred when the initial standard deviation was set to 0.5 (the same as the experiments presented in Figure 12).

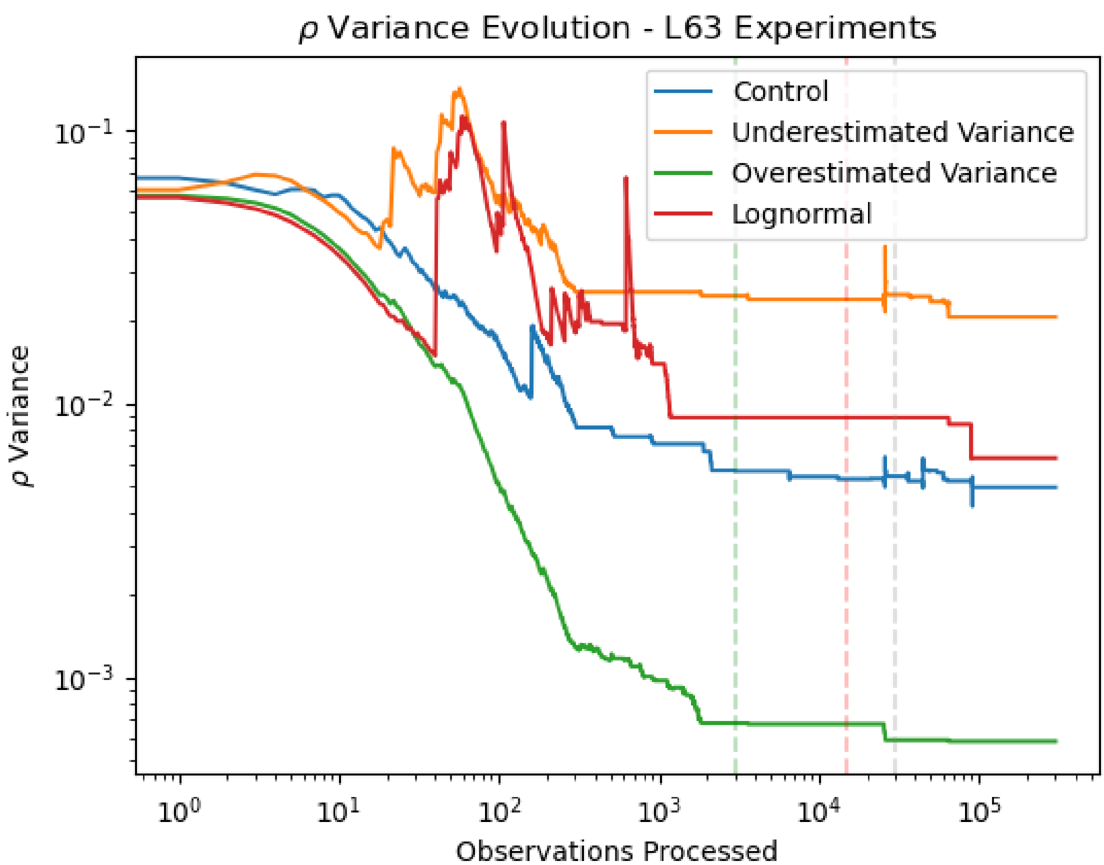

FIG. A1: Variances of the distributional estimate of ρ made by the ABIG scheme in four L63 experiments. The green, red, and grey dashed lines represent the 1000$^{\text{th}}$, 5000$^{\text{th}}$, and 10000$^{\text{th}}$ assimilation window, respectively.

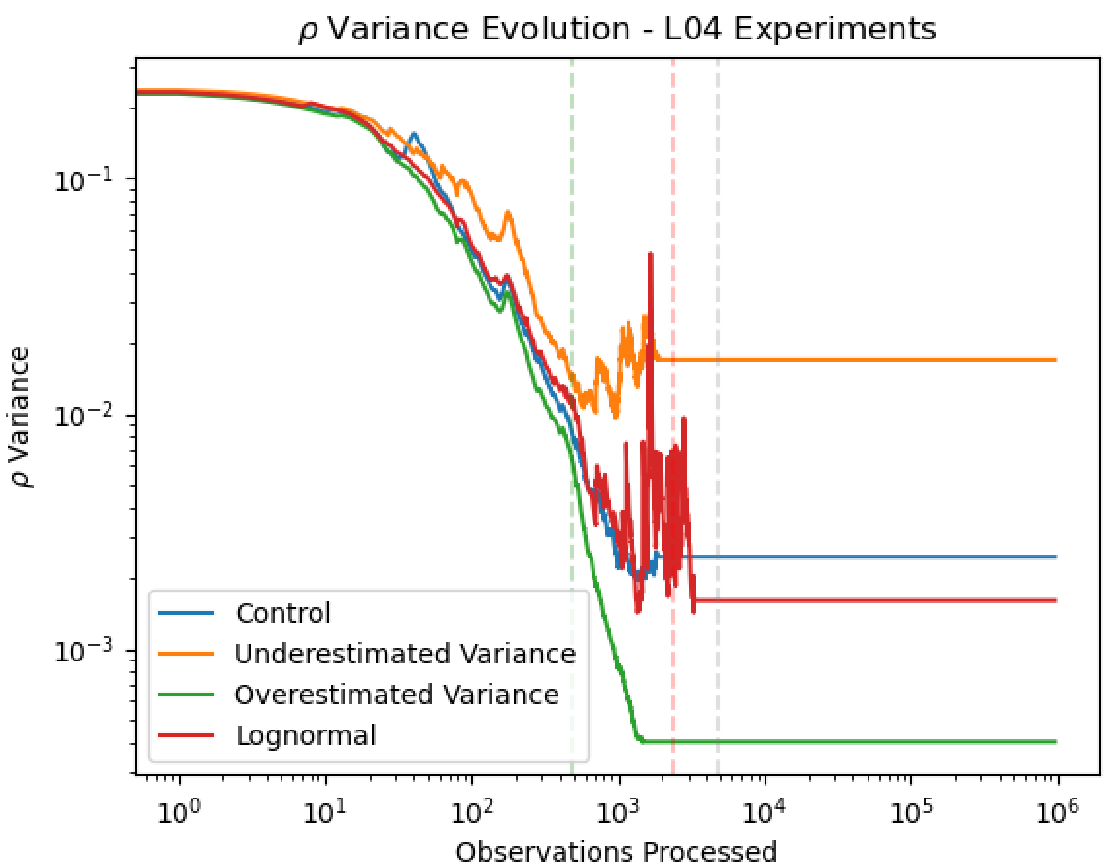

FIG. A2: As in Figure A1, but for L04 experiments. The green, red, and grey dashed lines represent the first, fifth, and tenth assimilation window, respectively.

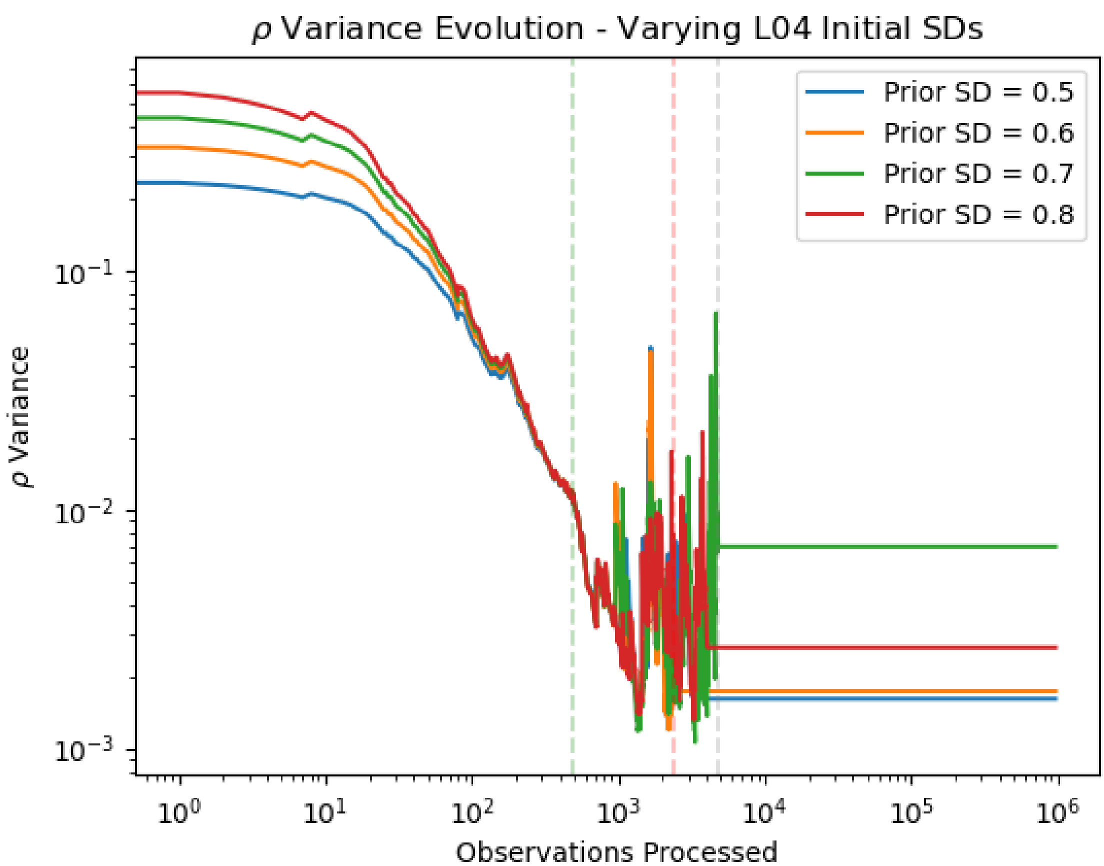

FIG. A3: Posterior variance evolution for log-normal error experiments with varying initial prior standard deviations. Dotted lines are as in Figure A3.

Acknowledgments. This research is funded by NSF Award AGS2136969. Special thanks to Jeff Anderson, Helen Kershaw, and the rest of the DART team for their insights and guidance in adding observation variance estimation methods to DART.

Data availability statement. All software and data used to generate results for this study is available upon request from the corresponding author.

References

Anderson, J. L., 2001: An Ensemble Adjustment Kalman Filter for Data Assimilation. URL https://journals.ametsoc.org/view/journals/mwre/129/12/1520-0493_2001_129_2884_aeakff_2.0.co_2.xml, section: Monthly Weather Review.

Anderson, J. L., 2009: Spatially and temporally varying adaptive covariance inflation for ensemble filters. *Tellus A*, **61 (1)**, 72–83, https://doi.org/10.1111/j.1600-0870.2008.00361.x, URL https://onlinelibrary.wiley.com/doi/abs/10.1111/j.1600-0870.2008.00361.x, _eprint: https://onlinelibrary.wiley.com/doi/pdf/10.1111/j.1600-0870.2008.00361.x.

Anderson, J. L., and N. Collins, 2007: Scalable Implementations of Ensemble Filter Algorithms for Data Assimilation. https://doi.org/10.1175/JTECH2049.1, URL https://journals.ametsoc.org/view/journals/atot/24/8/jtech2049_1.xml, section: Journal of Atmospheric and Oceanic Technology.

Bishop, C. H., 2016: The GIGG-EnKF: ensemble Kalman filtering for highly skewed non-negative uncertainty distributions. *Quarterly Journal of the Royal Meteorological Society*, **142 (696)**, 1395–1412, https://doi.org/10.1002/qj.2742, URL https://onlinelibrary.wiley.com/doi/abs/10.1002/qj.2742, _eprint: https://onlinelibrary.wiley.com/doi/pdf/10.1002/qj.2742.

Bishop, C. H., 2019: Data assimilation strategies for state-dependent observation error variances. *Quarterly Journal of the Royal Meteorological Society*, **145 (718)**, 217–227, https://doi.org/10.1002/qj.3424, URL https://onlinelibrary.wiley.com/doi/abs/10.1002/qj.3424, _eprint: https://onlinelibrary.wiley.com/doi/pdf/10.1002/qj.3424.

Bormann, N., and P. Bauer, 2010: Estimates of spatial and interchannel observation-error characteristics for current sounder radiances for numerical weather prediction. I: Methods and application to ATOVS data. *Quarterly Journal of the Royal Meteorological Society*, **136 (649)**, 1036–1050, https://doi.org/10.1002/qj.616, URL https://onlinelibrary.wiley.com/doi/abs/10.1002/qj.616, _eprint: https://onlinelibrary.wiley.com/doi/pdf/10.1002/qj.616.

Campbell, W. F., E. A. Satterfield, B. Ruston, and N. L. Baker, 2017: Accounting for Correlated Observation Error in a Dual-Formulation 4D Variational Data Assimilation System.

https://doi.org/10.1175/MWR-D-16-0240.1, URL https://journals.ametsoc.org/view/journals/mwre/145/3/mwr-d-16-0240.1.xml, section: Monthly Weather Review.

Chandramouli, K., X. Wang, A. Johnson, and J. Otkin, 2022: Online Nonlinear Bias Correction in Ensemble Kalman Filter to Assimilate GOES-R All-Sky Radiances for the Analysis and Prediction of Rapidly Developing Supercells. *Journal of Advances in Modeling Earth Systems*, **14 (3)**, e2021MS002 711, https://doi.org/10.1029/2021MS002711, URL https://onlinelibrary.wiley.com/doi/abs/10.1029/2021MS002711, _eprint: https://onlinelibrary.wiley.com/doi/pdf/10.1029/2021MS002711.

Dee, D., 1997: On-Line Estimation of Error Covariance Parameters for Atmospheric Data Assimilation. *Monthly Weather Review*, **123**, https://doi.org/10.1175/1520-0493(1995)123⟨1128:OLEOEC⟩2.0.CO;2.

Desroziers, G., L. Berre, B. Chapnik, and P. Poli, 2005: Diagnosis of observation, background and analysis-error statistics in observation space. *Quarterly Journal of the Royal Meteorological Society*, **131 (613)**, 3385–3396, https://doi.org/10.1256/qj.05.108, URL https://onlinelibrary.wiley.com/doi/abs/10.1256/qj.05.108, _eprint: https://onlinelibrary.wiley.com/doi/pdf/10.1256/qj.05.108.

Desroziers, G., and S. Ivanov, 2001: Diagnosis and adaptive tuning of observation-error parameters in a variational assimilation. *Quarterly Journal of the Royal Meteorological Society*, **127 (574)**, 1433–1452, https://doi.org/10.1002/qj.49712757417, URL https://onlinelibrary.wiley.com/doi/abs/10.1002/qj.49712757417, _eprint: https://onlinelibrary.wiley.com/doi/pdf/10.1002/qj.49712757417.

Gharamti, M. E., 2018: Enhanced Adaptive Inflation Algorithm for Ensemble Filters. *Monthly Weather Review*, **146 (2)**, 623–640, https://doi.org/10.1175/MWR-D-17-0187.1, URL https://journals.ametsoc.org/view/journals/mwre/146/2/mwr-d-17-0187.1.xml, publisher: American Meteorological Society Section: Monthly Weather Review.

Hu, C.-C., P. J. van Leeuwen, and A. J. Geer, 2024: A non-parametric way to estimate observation errors based on ensemble innovations. *Quarterly Journal of the Royal Meteorological Society*, **150 (761)**, 2296–2315, https://doi.org/10.1002/qj.4710, URL https://onlinelibrary.wiley.com/doi/abs/10.1002/qj.4710, _eprint: https://onlinelibrary.wiley.com/doi/pdf/10.1002/qj.4710.

Janjić, T., and Coauthors, 2018: On the representation error in data assimilation. *Quarterly Journal of the Royal Meteorological Society*, **144 (713)**, 1257–1278, https://doi.org/10.1002/qj.3130, URL https://onlinelibrary.wiley.com/doi/abs/10.1002/qj.3130, _eprint: https://onlinelibrary.wiley.com/doi/pdf/10.1002/qj.3130.

Karspeck, A. R., 2016: An Ensemble Approach for the Estimation of Observational Error Illustrated for a Nominal 1° Global Ocean Model. *Monthly Weather Review*, **144 (5)**, 1713–1728, https://doi.org/10.1175/MWR-D-14-00336.1, URL https://journals.ametsoc.org/view/journals/mwre/144/5/mwr-d-14-00336.1.xml, publisher: American Meteorological Society Section: Monthly Weather Review.

Knisely, J., and J. Poterjoy, 2023: Implications of Self-Contained Radiance Bias Correction for Data Assimilation within the Hurricane Analysis and Forecasting System (HAFS). https://doi.org/10.1175/WAF-D-23-0027.1, URL https://journals.ametsoc.org/view/journals/wefo/38/9/WAF-D-23-0027.1.xml, section: Weather and Forecasting.

Kotsuki, S., T. Miyoshi, K. Terasaki, G.-Y. Lien, and E. Kalnay, 2017: Assimilating the global satellite mapping of precipitation data with the Nonhydrostatic Icosahedral Atmospheric Model (NICAM). *Journal of Geophysical Research: Atmospheres*, **122 (2)**, 631–650, https://doi.org/10.1002/2016JD025355, URL https://onlinelibrary.wiley.com/doi/abs/10.1002/2016JD025355, _eprint: https://onlinelibrary.wiley.com/doi/pdf/10.1002/2016JD025355.

Li, H., E. Kalnay, and T. Miyoshi, 2009: Simultaneous estimation of covariance inflation and observation errors within an ensemble Kalman filter. *Quarterly Journal of the Royal Meteorological Society*, **135 (639)**, 523–533, https://doi.org/10.1002/qj.371, URL https://onlinelibrary.wiley.com/doi/abs/10.1002/qj.371, _eprint: https://onlinelibrary.wiley.com/doi/pdf/10.1002/qj.371.

Lorenz, E. N., 1963: Deterministic Nonperiodic Flow. *Journal of the Atmospheric Sciences*, URL https://journals.ametsoc.org/view/journals/atsc/20/2/1520-0469_1963_020_0130_dnf_2_0_co_2.xml, section: Journal of the Atmospheric Sciences.

Lorenz, E. N., 2005: Designing Chaotic Models. *Journal of the Atmospheric Sciences*, https://doi.org/10.1175/JAS3430.1, URL https://journals.ametsoc.org/view/journals/atsc/62/5/jas3430.1.xml, section: Journal of the Atmospheric Sciences.

Miyoshi, T., E. Kalnay, and H. Li, 2013: Estimating and including observation-error correlations in data assimilation. *Inverse Problems in Science and Engineering*, **21 (3)**, 387–398, https://doi.org/10.1080/17415977.2012.712527, URL https://doi.org/10.1080/17415977.2012.712527, publisher: Taylor & Francis _eprint: https://doi.org/10.1080/17415977.2012.712527.

Ménard, R., Y. Yang, and Y. Rochon, 2009: Convergence and stability of estimated error variances derived from assimilation residuals in observation space.

Semane, N., R. Anthes, J. Sjoberg, S. Healy, and B. Ruston, 2022: Comparison of Desroziers and Three-Cornered Hat Methods for Estimating COSMIC-2 Bending Angle Uncertainties. https://doi.org/10.1175/JTECH-D-21-0175.1, URL https://journals.ametsoc.org/view/journals/atot/39/7/JTECH-D-21-0175.1.xml, section: Journal of Atmospheric and Oceanic Technology.

Stroud, J. R., and T. Bengtsson, 2007: Sequential State and Variance Estimation within the Ensemble Kalman Filter. *Monthly Weather Review*, **135 (9)**, 3194–3208, https://doi.org/10.1175/MWR3460.1, URL https://journals.ametsoc.org/view/journals/mwre/135/9/mwr3460.1.xml, publisher: American Meteorological Society Section: Monthly Weather Review.

Stroud, J. R., M. Katzfuss, and C. K. Wikle, 2018: A Bayesian Adaptive Ensemble Kalman Filter for Sequential State and Parameter Estimation. *Monthly Weather Review*, **146 (1)**, 373–386, https://doi.org/10.1175/MWR-D-16-0427.1, URL https://journals.ametsoc.org/view/journals/mwre/146/1/mwr-d-16-0427.1.xml, publisher: American Meteorological Society Section: Monthly Weather Review.

Tandeo, P., P. Ailliot, M. Bocquet, A. Carrassi, T. Miyoshi, M. Pulido, and Y. Zhen, 2020: A Review of Innovation-Based Methods to Jointly Estimate Model and Observation Error Covariance Matrices in Ensemble Data Assimilation. https://doi.org/10.1175/MWR-D-19-0240.1, URL https://journals.ametsoc.org/view/journals/mwre/148/10/mwrD190240.xml, section: Monthly Weather Review.

UCAR/NSF NCAR/CISL/DAReS, 2024: The Data Assimilation Research Testbed (version 10.7.3) [software]. URL https://github.com/NCAR/DART, https://doi.org/10.5065/D6WQ0202.

Walsworth, A., J. Poterjoy, and E. Satterfield, 2023: Challenges for Inline Observation Error Estimation in the Presence of Misspecified Background Uncertainty. *Monthly Weather*

Review, https://doi.org/10.1175/MWR-D-22-0298.1, URL https://journals.ametsoc.org/view/journals/mwre/151/9/MWR-D-22-0298.1.xml, section: Monthly Weather Review.